Gas-Phase Specific Reactivity of Isomeric 1,3-Benzodithiole Anions: Tandem Mass Spectrometry and DFT Theoretical Studies

Yves Gimbert,*,† Roger Arnaud,*,‡ Edmond de Hoffman,§ and J. C. Tabet||

Université Joseph Fourier de Grenoble, Chimie Recherche - Equipe de Synthèse Organique (LEDSS), 38041 Grenoble Cedex, France, Université Joseph Fourier de Grenoble, Chimie Recherche - Equipe de Chimie Théorique (LEDSS), 38041 Grenoble Cedex, France, Université Catholique de Louvain, Laboratoire de Spectrométrie de Masse, Place Pasteur, 1, B-1348 Louvain la Neuve, Belgique, and Université Pierre et Marie Curie, Laboratoire de Chimie Structurale Organique et Biologique, 4, Place Jussieu, 75230 Paris Cedex 05, France

Received: September 15, 2000; In Final Form: February 9, 2001

1,3-Benzodithiole dideuterated at the dithioacetal carbon atom has been ionized in the chemical ionization source of a tandem triple quadrupole mass spectrometer under NICI condition. Two isomeric anions are formed by abstraction of an *o*-phenylic proton or through abstraction of a deuteron. The fragmentation patterns occurring under dissociative collisions differ and confirm the coexistence of two nonconverting carbanions. DFT calculations show that the dithioacetal anion is more stable than the phenylic. The nucleophilic reactivity toward CS_2 has been studied by collision-induced reactions in the collision cell of the tandem instrument. Both isomeric anion forms display characteristic fragmentations of the resulting $[(M-H(D)) + CS_2]$ adduct anions, demonstrating a difference in reactivity: the dithioacetal anion reacts regioselectively at C and the *o*-phenylic at S. DFT calculations, performed with the aim of rationalizing this observed difference and understanding the formation of the diagnostic fragments, have been successful.

Introduction

The continuing interest in the experimental reactivity (unimolecular and bimolecular processes) and fundamental properties of anions derived from organosulfur compounds is due to their importance in synthetic organic chemistry.[1] The particular reactivity of sulfur-containing anions differs from that characterizing the analogous oxygen-containing compounds. The mechanism of the stabilization of the negative charge on a carbon atom adjacent to a third-row element—especially sulfur—has been a matter of discussion. On the basis of PMO theory, interaction between the carbanion lone pair and the antibonding σ^* orbital of the S−R group has been suggested to contribute to the stabilization of the carbanion site.[2] It is well established that this stabilization by third-row substituents is due mainly to polarization and negative hyperconjugation and not to d-orbital effects, as suggested in a few publications. Carbanions derived from thioacetals are widely used in organic chemistry as masked acyl anion equivalents,[3] mainly with 1,3-dithiane, in contrast to the carbanion derived from dithiolane which has been described as impossible to produced because of immediate decomposition into ethylene and dithioformate anion. Other such anions, such as 2-lithio-1,3-benzodithioles ($\mathbf{1}_{Li}$, Scheme 1), have also been recommended as masked acyl anions.[4,5] In addition to reversing the carbonyl group reactivity, anions from 1,3-dithioles are also very useful as building blocks for new sulfur heterocycles. Researchers have investigated[6,7] the reactions of these species with CS_2 as a way to an interesting synthon and a redox-active ligand (Scheme 1).

SCHEME 1

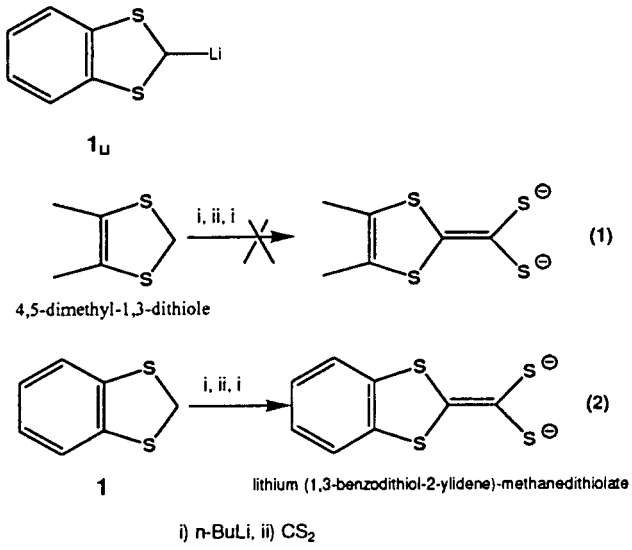

Surprisingly, the anion from 4,5-dimethyl-1,3-dithiole does not react with carbon disulfide in the predicted way (eq 1).[6] On the other hand, under the same conditions (Scheme 1, eq 2), the anion from 1,3-benzodithiole **1** leads to the expected dianion, lithium (1,3-benzodithiol-2-ylidene)methanedithiolate.[7] This dramatic difference in the reaction with CS_2 of these apparently similar dithioles led us to investigate a series of 1,3-dithioles in order to gain some insight into the relationship between the structure of the dithiole carbanion and its reactivity

* Corresponding authors. Tel: (33) 4-76-51-46-91. Fax: (33) 4-76-51-43-82. E-mail: Yves.Gimbert@ujf-grenoble.fr (Y.G.) and Roger.Arnaud@ujf-grenoble.fr (R.A.).

† Université Joseph Fourier de Grenoble, Chimie Recherche - Equipe de Synthèse Organique (LEDSS).

‡ Université Joseph Fourier de Grenoble, Chimie Recherche - Equipe de Chimie Théorique (LEDSS).

§ Université Catholique de Louvain.

|| Université Pierre et Marie Curie.

10.1021/jp003294j CCC: $20.00 © 2001 American Chemical Society
Published on Web 05/05/2001

CHART 1

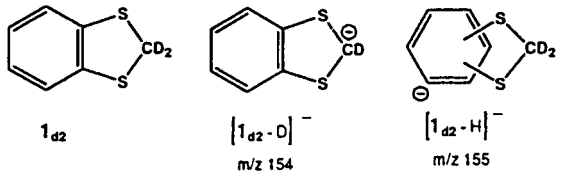

toward carbon disulfide and the nature of the initially formed reaction intermediates. The experimentally obtained information on the properties of α-thiocarbanions produced from dithioacetals and dithioles has been derived nearly exclusively from solution studies. However, these carbanions do not exist as free ions in solution but as the corresponding organometallic compounds. To observe them free from solvent and counterion effects, we must generate them in the gas phase.[8] Significantly, it has been repeatedly shown by the observed behavior of gas-phase carbanions that the reaction mechanisms developed can be successfully applied with only minor variation to the corresponding species in solution.[9] In this paper, we report for the first time the two gas-phase structures of the 1,3-benzodithiole $\mathbf{1}_{d2}$ anions produced in a chemical ionization high-pressure source and their regioselective reactions toward CS_2. DFT calculations (using the hybrid functional B3LYP) for each 1,3-benzodithiole anion and their ion−molecule reactions with CS_2 are also described.

Experimental Section Part

Mass Spectrometry. All experiments were carried out on a triple quadrupole Finnigan TSQ 70 instrument, which has been previously described.[8b] The 1,3-benzodithiole bisdeuterated at C_2 (prepared by reduction using $LiAlD_4$ of the known corresponding trithiocarbonate), $\mathbf{1}_{d2}$ (Chart 1), was deprotonated under Negative Ion Chemical Ionization conditions in the high-pressure source at 0.8 Torr (using a 75%/25% CH_4/N_2O reagent gas mixture).

The high-pressure source was operated under the following NICI conditions: 100 eV electron energy, 0 V repeller, and 50 mA electron current. From the selected main beam, dissociative collisions (as collison-induced dissociation (CID) spectra) and ion−molecule reaction experiments (as collision-activated reaction (CAR) spectra) were performed in the collision cell. $[M-H(D)]^-$ anions were submitted to low collision energy processes (i.e., E_{lab} varied from 2 to 10 eV): (i) dissociative pathways with the Xe target (at 0.8 mTorr, uncorrected gauge reading) and (ii) ion−molecule reactions (partially associated with dissociation pathways) induced by the electrophilic CS_2 reagent introduced into the collision cell (at 3 mTorr). Alternatively, the study of the reactions produced by a selected natural ^{34}S labeled anion provided the origin of the sulfur atoms present in the anions generated in ion−molecule reactions. To prepare in the ion source a stable $[(M-H(D)) + CS_2]^-$ adduct anion, we introduced benzodithiole $\mathbf{1}_{d2}$ and CS_2 together into the CI source and placed xenon in the collision cell to perform adduct ion dissociation. In this way, $[(M-H(D)) + CS_2]^-$ adduct ions with different isotopic compositions were generated in the source. One of them selected by the MS1 analyzer was dissociated by collision. This allowed the acquisition of structural information concerning the "survivor" adduct $[(M-H(D)) + CS_2]^-$ anions, which was compared with that obtained from further decompositions of adduct anions prepared in the collision cell by collision induced reaction with the electrophilic CS_2 reagent.

Computational Details

Density functional calculations were carried out within the Kohn−Sham (KS) formalism, as implemented in the Gaussian 98 code.[10] We have chosen the so-called B3LYP computational model, a self-consistent hybrid approach[11] obtained by a mixture of HF exchange and DFT exchange-correlation[12] using the Lee, Yang, and Parr correlation functional.[13] All the molecular stuctures have been fully optimized using the 6-31+G(d) basis set; spin-restricted B3LYP calculations were performed on the reactants and most of the intermediates and transition states; unrestricted UB3LYP calculations were carried out in some cases to check for the possible intermediacy of diradicals and diradical characters leading to them. Corrections for differences in zero-point vibrational energies (ZPE) were calculated from unscaled vibrational frequencies at the (U)B3LYP/6-31+G(d) level. Basis set truncation effects were further investigated by B3LYP single-point calculations using the 6-311+G(2df,2p) basis set.

We have also performed a natural population analysis (NPA),[14] which yields reliable atomic charges[15] and natural bond orbital (NBO)[14] calculations, to analyze some delocalization interactions and to provide a chemical description of the bonding in terms of interactions between localized hybrid orbitals.

Results

Mass spectra Experiments. *1. Formation of the $[\mathbf{1}_{d2}-D]^-$ and $[\mathbf{1}_{d2}-H]^-$ Deprotonated Molecules.* The NICI of $\mathbf{1}_{d2}$ with CH_4/N_2O results in the formation of *m/z* 154 and *m/z* 155 peaks, arising from an abstraction of D and H, respectively. The intensities of the *m/z* 154 and *m/z* 155 peaks are 51% and 12%, respectively, of the peak at *m/z* 96 (base peak in the -Q1MS spectrum). The peak at *m/z* 155 is mainly $[\mathbf{1}_{d2}-H]^-$, contaminated by the natural isotopic ^{13}C ($1.1\% \times 7/0.23 = 33\%$) and ^{33}S ($0.75\% \times 2/0.23 = 6.5\%$) contributions of the *m/z* 154 anion. Thus, a priori, 39% of the *m/z* 155 peak intensity results from natural isotopes of ions at *m/z* 154, with the remainder (> 60%) attributed to the isobaric $[\mathbf{1}_{d2}$ - H$]^-$ ions.

2. CID Spectra of the Different $[\mathbf{1}_{d2}-D]^-$ and $[\mathbf{1}_{d2}-H]^-$ anions. The selected $[\mathbf{1}_{d2}-D]^-$ (*m/z* 154) and $[\mathbf{1}_{d2}-H]^-$ (*m/z* 155) deprotonated molecules were submitted to low-energy collisions ($E_{lab} = 4$ eV, with xenon as the target) to produce the CID spectra shown in Figure 1. To assign the elemental compositions of these daughter ions, we made comparison with the CID obtained from the same ions, in which a ^{34}S was selected (*m/z* = 156). Concerning the $[\mathbf{1}_{d2}-D]^-$ ions, the peak at *m/z* 78 is shifted to *m/z* 80 in the CID of $[\mathbf{1}_{d2}(^{34}S) - D]^-$ (*m/z* 156), which reflects the presence in this ion of the two sulfur atoms of the starting anion, while the peak at *m/z* 110 is partially shifted to *m/z* 112 in a 50/50 ratio, which reflects that only one sulfur atom from the starting anion is present in this ion. Concerning the$[\mathbf{1}_{d2}-H]^-$ ions, *m/z* 57 and 107 are partially shifted to *m/z* 59 and 109, which reflects the fact that these ions contain only one sulfur atom of the starting anion at *m/z* 155. Elemental compositions are indicated in Figure 1.

From this CID spectrum, it can noted that the $[\mathbf{1}_{d2}-D]^-$ *m/z* 154 (51%) yields two specific fragment ions at *m/z* 78 (100%) and 110 (28%). The $[\mathbf{1}_{d2}-H]^-$ *m/z* 155 (100%) also displays typical fragment ions at *m/z* 57 (7%) and 107 (20%). The ions observed at *m/z* 78/79 and 110/111 only result from the ^{13}C and ^{33}S contributions to *m/z* 155 of the *m/z* 154 anion.

3. Ions Produced by Ion−Molecule Reactions of $[\mathbf{1}_{d2}-D]^-$ and $[\mathbf{1}_{d2}-H]^-$ with CS_2 as the Electrophile in the Collision Cell. The CAR spectra of the selected $[\mathbf{1}_{d2}-D]^-$ and $[\mathbf{1}_{d2}-H]^-$ anions with the neutral CS_2 reagent were investigated and reported in

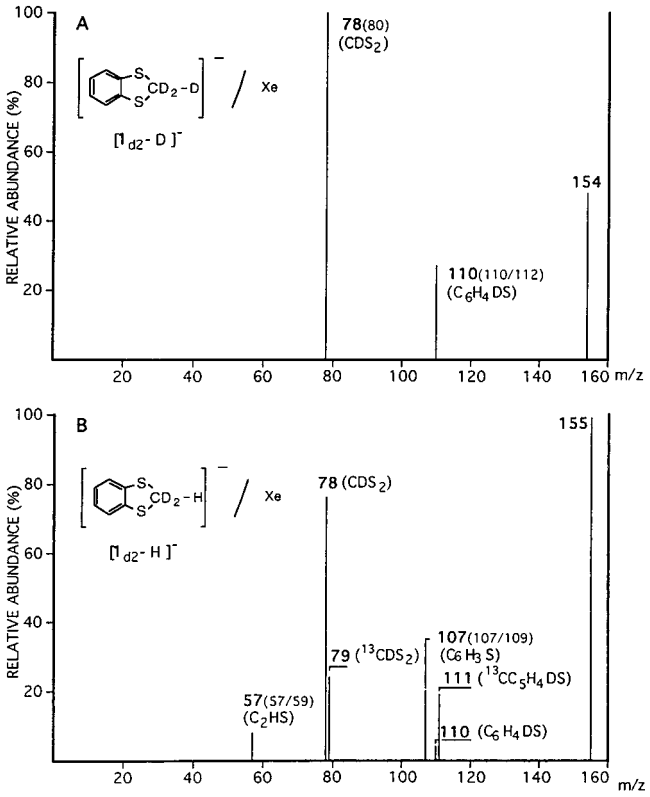

Figure 1. (A) Collision-induced dissociation (CID) spectrum of $[\mathbf{1}_{d2}-D]^-$ (xenon target gas, $E_{lab} = 4$ eV). (B) CID spectrum of $[\mathbf{1}_{d2}-H]^-$ (xenon target gas, $E_{lab} = 4$ eV).

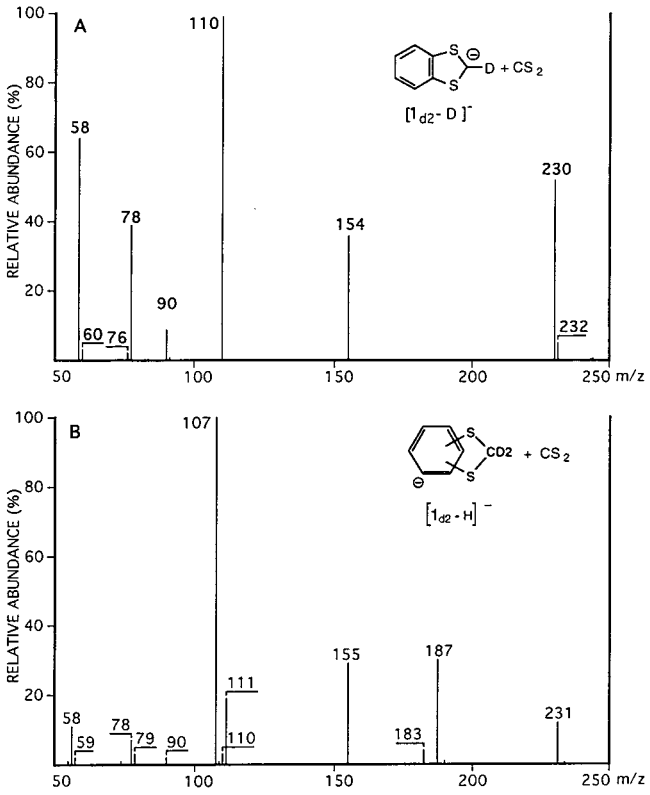

Figure 2. (A) Reactive collision spectra under low collision energy conditions of $[\mathbf{1}_{d2}-D]^-$ (CS_2 target gas, $E_{lab} = 3$ eV). (B) Reactive collision spectra under low collision energy conditions of $[\mathbf{1}_{d2}-D]^-$ (CS_2 target gas, $E_{lab} = 3$ eV)

panels A and B, repectively, of Figure 2. Specific fragmentations of the adduct $\{[\mathbf{1}_{d2}-D] + CS_2\}^-$ (*m*/*z* 230) and $\{[\mathbf{1}_{d2}-H] + CS_2\}^-$ (*m*/*z* 231) ions are observed. The sulfur atom coming

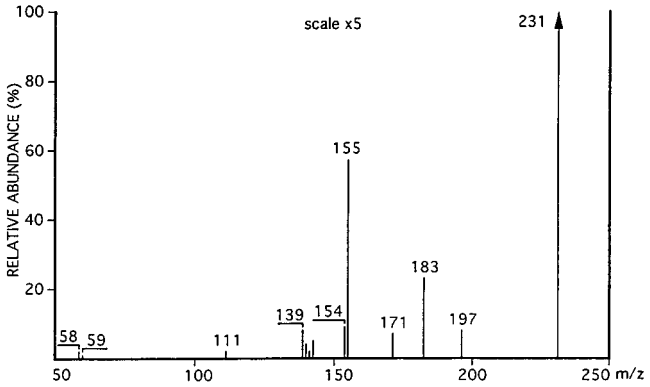

Figure 3. CID spectrum of $[(\mathbf{1}_{d2}-H]) + CS_2]^-$ (xenon target gas, $E_{lab} = 4$ eV).

from CS_2 is indicated in italics.[16] Concerning the ion *m*/*z* 230, the specific peaks are *m*/*z* 90 (10%)(C_2DSS^-) and *m*/*z* 58 (64%)(C_2DS^-). The adduct at *m*/*z* 231 gives specific fragment ions at *m*/*z* 187 (29%) ($C_7H_3D_2S_2S^-$) and *m*/*z* 183 (5%) ($C_7H_3SS_2^-$).

Finally, the $\{[\mathbf{1}_{d2}-D] + CS_2\}^-$ and $\{[\mathbf{1}_{d2}-H] + CS_2\}^-$ adducts could be formed in the chemical ionization source, after introduction of the benzodithiole $\mathbf{1}_{d2}$ and CS_2 together in CH_4/N_2O ionization plasma. In this way, the adduct ions at *m*/*z* 230 and 231 were successively selected as parent ions and fragmented using xenon as the collision gas. This allowed the direct observation of their fragmentation products. The CID spectrum of$\{[\mathbf{1}_{d2}-D] + CS_2\}^-$ did not present significative differences compared to the CID spectrum shown in Figure 2A. In contrast, by comparison with the CAR spectrum shown in Figure 2B, the CID spectrum obtained from $\{[\mathbf{1}_{d2}-H] + CS_2\}^-$ (Figure 3) indicated the disappearance of the *m*/*z* 187 ion and many abundance changes. Indeed, the " survivor " *m*/*z* 231 ions from ion source are stable when they are produced in the CI source and decompose under collision conditions into fragment *m*/*z* 183 ions by loss of CD_2S.

Discussion

A. Deprotonation site of 1,3-Benzodithiole: Comparison of the CID Spectra of the Isomeric $[\mathbf{1}_{d2}-D]^-$ and $[\mathbf{1}_{d2}-H]^-$ Anions to Low-Energy Processes. 1,3-Benzodithiole contains four different acidic sites: the dithioacetal carbon atom and the aromatic positions. To differentiate the aromatic positions from the dithioacetal site, we have employed 1,3-benzodithiole bisdeuterated at C2. The clear-cut specificity of the fragmentation of the isomeric $[\mathbf{1}_{d2}-D]^-$ and $[\mathbf{1}_{d2}-H]^-$ anions demonstrates that these isomeric anions do not interconvert; their fragmentation pathways clearly depend on the location of the charge.[17] Nevertheless, an ambiguity remains: does the deprotonation on the benzodithiole ring occur at an ortho or meta site or both? On the basis of analogy with Nibbering's work with thioanisole,[18a] the assumption can be made that deprotonation occurs at an ortho position. More recently, other study concerning to the acidity of ortho position of thiofunctionalized derivatives has been investigated during $[M-H]^-$ dissociation,[18b] but at this stage of the study, it is still just an assumption and we cannot overlook the possibility of meta deprotonation (see theoretical discussion).

The fragmentation spectra of the two isomeric anions are displayed in Figure 1. Elemental composition has been discussed before. Possible mechanisms for the formation of these ions are presented in Scheme 2:

(i) The dithioacetal $[\mathbf{1}_{d2}-D]^-$ anion (*m*/*z* 154) leads to the

SCHEME 2

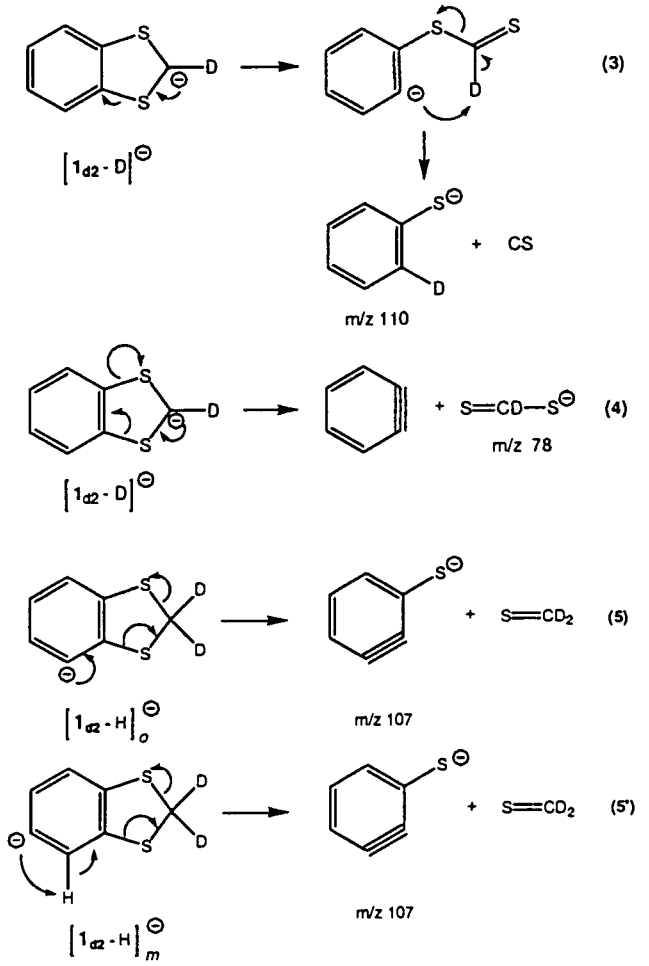

fragment $C_6H_4DS^-$ ion (*m*/*z* 110) retaining the deuterium by a ring-opening process through direct benzylic S−C bond cleavage, followed by a 1−4 deuteron migration (Scheme 2, eq 3). Such a cleavage may be considered to be a process competitive with phenyl ring cleavage with formation of S_2CD^- at *m*/*z* 78 (e.g., as S=CD−S$^-$ or isomeric structure) by loss of neutral benzyne, C_6H_4 (Scheme 2, eq 4). Note that neutral loss from the dithioacetal anion by direct cycloreversion (induced by a negative charge at the dithioacetal position) can be considered similar to the C_2H_4 elimination observed from decomposition of the dithioacetal anion prepared by deprotonation of 1,3-dithiolane.[8a]

(ii) The phenyl anions $[\mathbf{1}_{d2}-H]_o^-$ and/or $[\mathbf{1}_{d2}-H]_m^-$ decompose by a charge-promoted ring cleavage, followed by the loss of CD_2S, leading to the formation of the benzyne $C_6H_3S^-$ (*m*/*z* 107) (Scheme 2, eq 5 and eq 5′).

In conclusion, the observed differences in dissociation of the two dithioacetal and phenyl isomeric anionic forms at low energy CID indicate that these ions are not interconvertible through 1−4 proton transfer; thus, it is reasonable to compare results provided from reactive collision between the anionic forms of the benzodithiole and carbon disulfide.

B. Ion−Molecule Reactions between $[\mathbf{1}_{d2}-D]^-$ and $[\mathbf{1}_{d2}-H]^-$ Anions and CS_2. Different reagent anions[19] condense with carbon disulfide and may react with this neutral reagent on either carbon or sulfur. With a thiophilic attack, sulfur atom transfer can occur with concomitant loss of CS. For example, gas-phase adducts have been observed between H_3Si^- and CS_2 by Sheldon and co-workers.[19d] Experiments by Squires and co-workers[19a,19c]

SCHEME 3

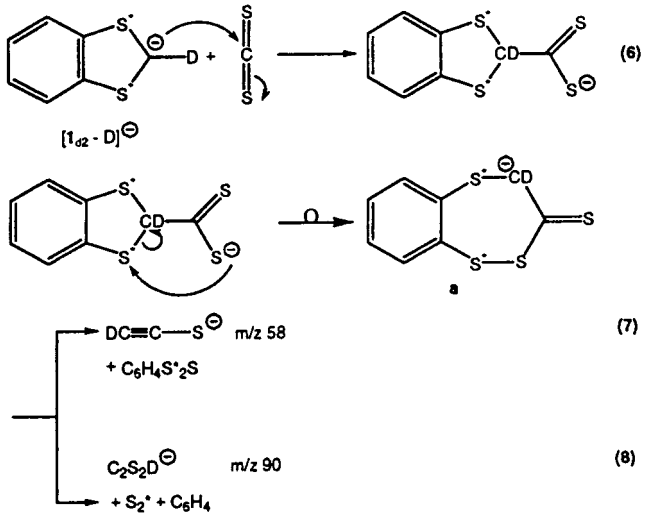

SCHEME 4

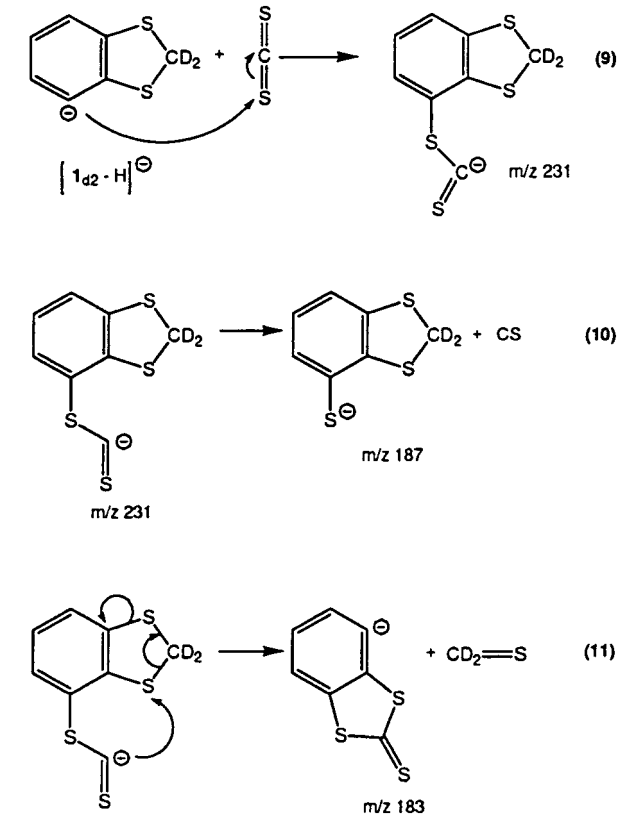

have produced CH_3S^- and $C_3H_5S^-$, the result of anion−molecule reaction between $CH_3^-/C_3H_5^-$ and CS_2. However, there is no example with anions derived from dithiole structures.

a. Reaction of the dithioacetal $[\mathbf{1}_{d2}-D]^-$ carbanion (m/z 154) with CS_2 produces a stable adduct ion (E_{lab} = 3 eV) by creation of a covalent bond. The absence in the CID spectrum (Figure 2A) of the *m*/*z* 186 ion corresponding to the loss of CS supports the idea that the nucleophilic attack is carbophilic. On the basis of this assumption, the fragmentation of the adduct ion should be in agreement with the thiolate structure as shown in Scheme 3, eq 6. Possible mechanisms explaining formation of these ions (elemental composition has been discussed above) are presented in Scheme 3 and will be discussed in the theoretical portion of this paper.

The formation of the *m*/*z* 90 and *m*/*z* 58 ions can be

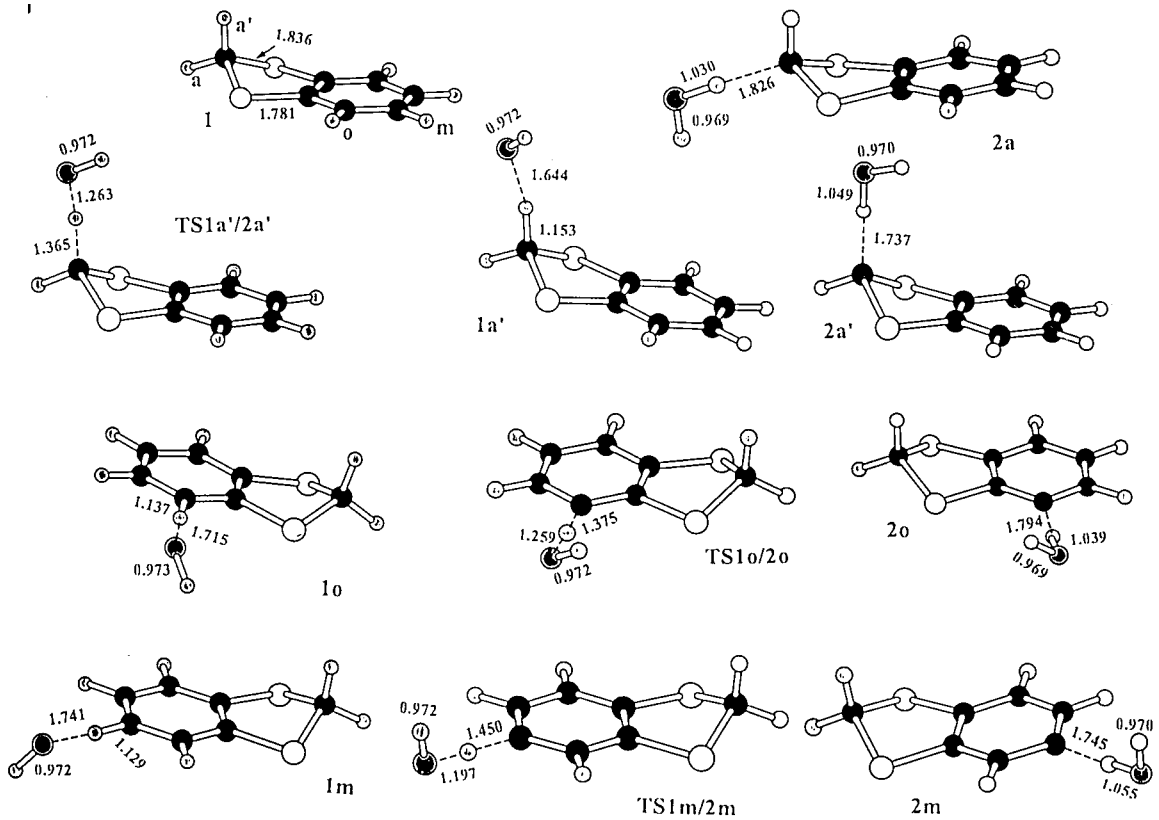

Figure 4. Optimized structures of the stationary points governing the deprotonation reaction of **1** by OH^-; the distances are in Å.

TABLE 1: Energies and Zero-Point Energies (relative to those of the reactants) for the Stationary Points on the Potential Surface of Deprotonation of 1 by OH^- and for the Nacked Anions (relative to 1)[a]

system[b]	ΔE[c]	ΔZPE	system[b]	ΔE[c]	ΔZPE
2a	−32.1 (−27.8)	0.4	**TS1m/2m**	−14.4 (−11.9)	−2.6
1a′	−20.8 (−19.9)	−0.1	**2m**	−15.5 (−13.3)	−0.2
TS1a′/2a′	−20.4 (−17.1)	−2.6			
2a′	−23.4 (−19.0)	−0.3	**3a**	0.0	0.0
1o	−18.5 (−18.6)	0.0	**3a′**	10.6	−0.5
TS1o/2o	−17.0 (−14.8)	−2.5	**TS3a/3a′**	11.6	−0.8
2o	−19.4 (−17.5)	−0.3	**3o*δ***	15.1	0.0
1m	−17.7 (−18.7)	0.1	**3m**	20.5	−0.1

[a] Energies in kcal/mol. [b] See Figures 4 and 5 for the nomenclature. [c] Single-point MP2 values in parentheses.

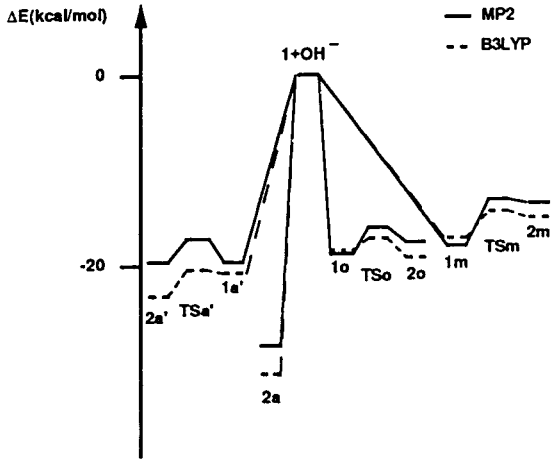

Figure 5. Deprotonation reaction of **1** by OH^- : scheme of the reaction profile at the B3LYP/6-311+G(2df,2p) and MP2/6-31+G(d) level of theory. The energies values are relative to those of the reactants.

rationalized by considering fragmentation of a common intermediate **a**, which may be formed by isomerization through rupture of a C−S bond of the initial adduct, to give the $C_2DS_2^-$ ion (*m*/*z* 90) by loss of $C_6H_4S_2$ and the C_2DS^- ion (*m*/*z* 58) by loss of $C_6H_4S_3^-$ (Scheme 3, eqs 8 and 7).

The adduct *m*/*z* 230 ion $\{[\mathbf{1}_{d2}-D] + CS_2\}^-$ is prepared in the high-pressure source (reagent mixture, $N_2O/CH_4/CS_2$). After selection by the first analyzer to be submitted to low energy dissociation collisions ($E_{lab} = 4$ eV) with xenon in the collision cell, this adduct decomposes into the same fragment ions as those produced from the *m*/*z* 154 ions submitted to reactive collisions with CS_2 in the cell also yielding a $\{[\mathbf{1}_{d2}-D] + CS_2\}^-$ adduct; thus, they can be considered to have a common structure.

b. Reaction of $[\mathbf{1}_{d2}-H]_o^-$ *and/or* $[\mathbf{1}_{d2}-H]_m^-$ with CS_2 produces an adduct $\{[\mathbf{1}_{d2}-H] + CS_2\}^-$ ion (*m*/*z* 231) that appears to be less stable than the form previously generated from $[\mathbf{1}_{d2}-D]^-$. The adduct ion gives fragment ions at *m*/*z* 187 and 183. Possible mechanisms for the formation of these ions (elemental composition has been discussed above) are presented in Scheme 4 and will be discussed in the theoretical part of this paper.

A thiophilic attack (Scheme 4, eq 9), rather than a carbophilic attack, is strongly suggested by the presence of ions at *m*/*z* 187, which corresponds to the loss of neutral CS from the adduct at *m*/*z* 231 (Scheme 4, eq 10). Furthermore, the $[\mathbf{1}_{d2}-H]_o^-$ carbanion form would seem to be preferred to the $[\mathbf{1}_{d2}-H]_m^-$ because from the adduct $\{[\mathbf{1}_{d2}-H]_o + CS_2\}^-$, the specific loss of CD_2S is reasonable: one sulfur atom from the 1−3 dithiole ring is lost, leading to the *m*/*z* 183 ($C_7H_3SS_2^-$) ion (Scheme 4, eq 11) (see theoretical studies).

While, as seen previously, there is no difference, from a fragmentation point of view, between the adduct *m*/*z* 230 prepared in the high pressure source and that prepared in the

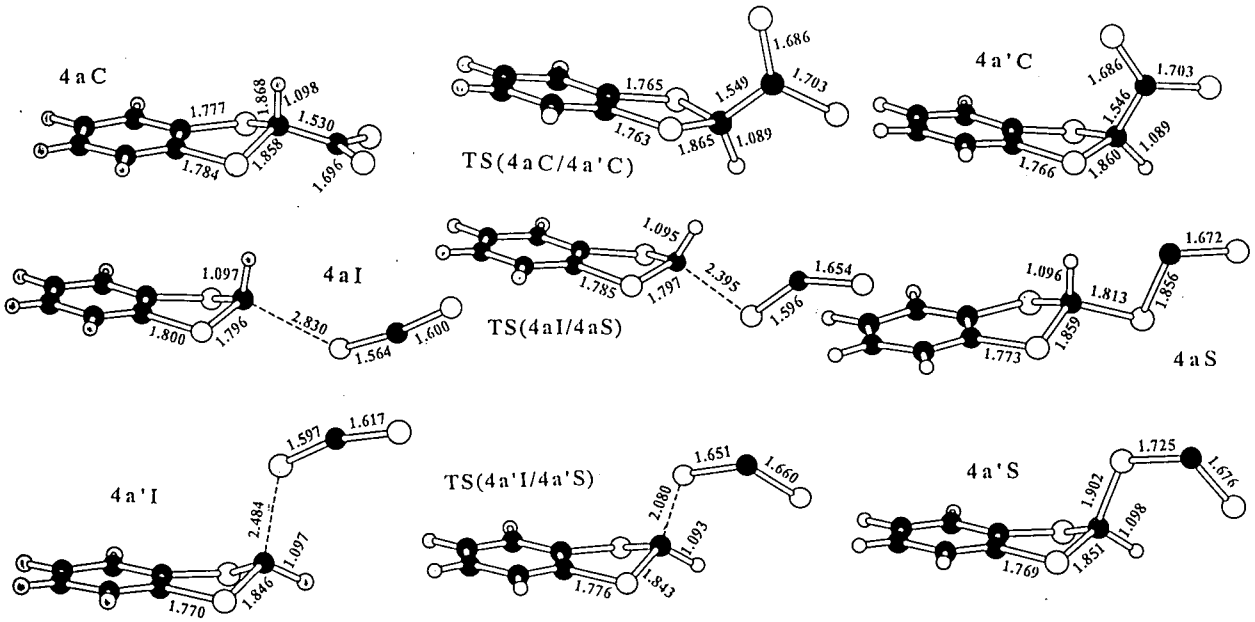

Figure 6. Optimized structures of the stationary points governing the **3a** (**3a′**) addition to CS_2; the distances are in Å.

TABLE 2: Energies and Zero-Point Energies (relative to those of the reactants) for the Stationary Points on the Potential Surface for 3a (3a′) Addition to CS_2 and for dissociation of addition products depicted in Figures 6 and 8[a]

systems	ΔE	ΔZPE	systems	ΔE	ΔZPE
			TS4aC/5	−16.0[b]	1.2
			TS4a′C/5	−21.0[c]	1.7
			5	−17.6[b]	1.9
4aC	−42.2[b]	2.7	**5′**	31.4[b]	−0.4
4a′C	−51.3[c]	3.5	**TS5/6**	−14.9[b]	1.9
4aI	−8.0[b]	0.5	**6**	−20.1[b]	2.2
TS4aI/4aS	13.1[b]	0.3	**TS6/7**	−1.6[b]	1.6
4aS	2.8[b]	1.2	**7**	−27.5[b]	2.0
4a′I	−12.5[c]	1.0	**TS7/8**	−3.4[b]	0.4
TS4a′I/4a′S	−10.2[c]	1.5	**8**	−12.8[b]	0.9
4a′S	−10.8[c]	1.7	**TS8/9**	17.0[b]	4.8
TS4aC/4a′C	−39.7[c]	1.1	**9**	13.6[b]	6.1

[a] Energies in kcal/mol. [b] Relative to **3a** + CS_2. [c] Relative to **3a′** + CS_2.

collision cell, this is not the case for the *m*/*z* 231 ion, whose fragmentation depends on its origin. Indeed, the "survivor" *m*/*z* 231 ions are stable when they are produced in the CI source and mainly decompose into the fragment *m*/*z* 183 ion by loss of CSD_2 (see Figure 3).

On the other hand, the adduct *m*/*z* 231 ion, produced in the collision cell, fragment into the *m*/*z* 187 ion, by loss of CS, in high abundance rather than by anion isomerization followed by loss of neutral CD_2S. This latter process is favored from the relaxed $\{ [\mathbf{1}_{d2}-H] + CS_2\}^-$ ions prepared in the ion source and submitted to dissociative collision.

The mass spectrometry results presented above and their interpretation require confirmation. At the same time, a number of questions are raised:

(i) Does the deprotonation on the ring in benzodithiole occur at the ortho or meta sites or both?

(ii) Is it possible that CS_2 reacts with phenide anions at C and under high energy conditions the resulting dithiolate anion then takes part in an intramolecular nucleophilic aromatic attack (through a three-membered ring) to yield a transient $Ar-SCS^-$ species?

(iii) Can the different reactivities of the two isomers $[\mathbf{1}_{d2}-H]^-$ and $[\mathbf{1}_{d2}-D]^-$ toward CS_2 be rationalized?

We have carried out DFT studies of the deprotonation reactions of the 1,3-benzodithiole system and of the reactions of the isomeric carbanions with CS_2 to seek answers to the questions above posed.

Theoretical Studies

A. Deprotonation of 1,3-Benzodithiole 1 by OH^-. Figure 4 displays B3LYP/6-31G(d) optimized geometries for the structures relevant to the proton transfer process in **1**; their relative energies are given in Table 1, and Figure 5 illustrates the potential energy profile.

On the basis of previous experience,[8b] all the geometry optimizations have been done at the B3LYP/6-31+G(d) level. Concerning proton-transfer reactions, B3LYP results have been compared to MP2/6-31+G(d) ones. Similar structures are obtained at these two levels of calculation; for intance, for **TS1o/2o**, optimized MP2 C−H, H−O, and O−H distances become 1.393, 1.242, and 0.976 Å, respectively (see Figure 4 for the corresponding B3LYP values).

Since the barrier heights and stabilization energies calculated in the framework of the supermolecule approach can be affected by the basis set superposition error (BSSE), we were prompted to examine BSSE in terms of the basis sets used; BSS corrections do not alter the relative energies and will be ignored in the following.[20] Table 1 and Figure 5 show that MP2/6-31G(d) energy barriers and reaction energies are higher than those of the B3LYP.[22] However, the two levels of calculation give similar trends. H_a transfer occurs without barrier and leads to the product complex **2a**; this process is very exothermic. For $H_{a'}$, H_o, and H_m transfers, the same mechanism has been found: first, formation of a reactant complex (**1a′**, **1o**, **1m**), followed by the formation of a product complex (**2a′**, **2o**, **2m**), these two complexes being separated by a weak energy barrier. In the reactant complexes, the O−H intermolecular distance parallels the stabilization energy: the shorter the distance is, the more stable the association will be. This behavior does not appear in product complexes. The product-like character of TS's, in accordance with the Hammond postulate, increases when the exothermicity of the **1** → **2** step decreases: thus, it is in the TS

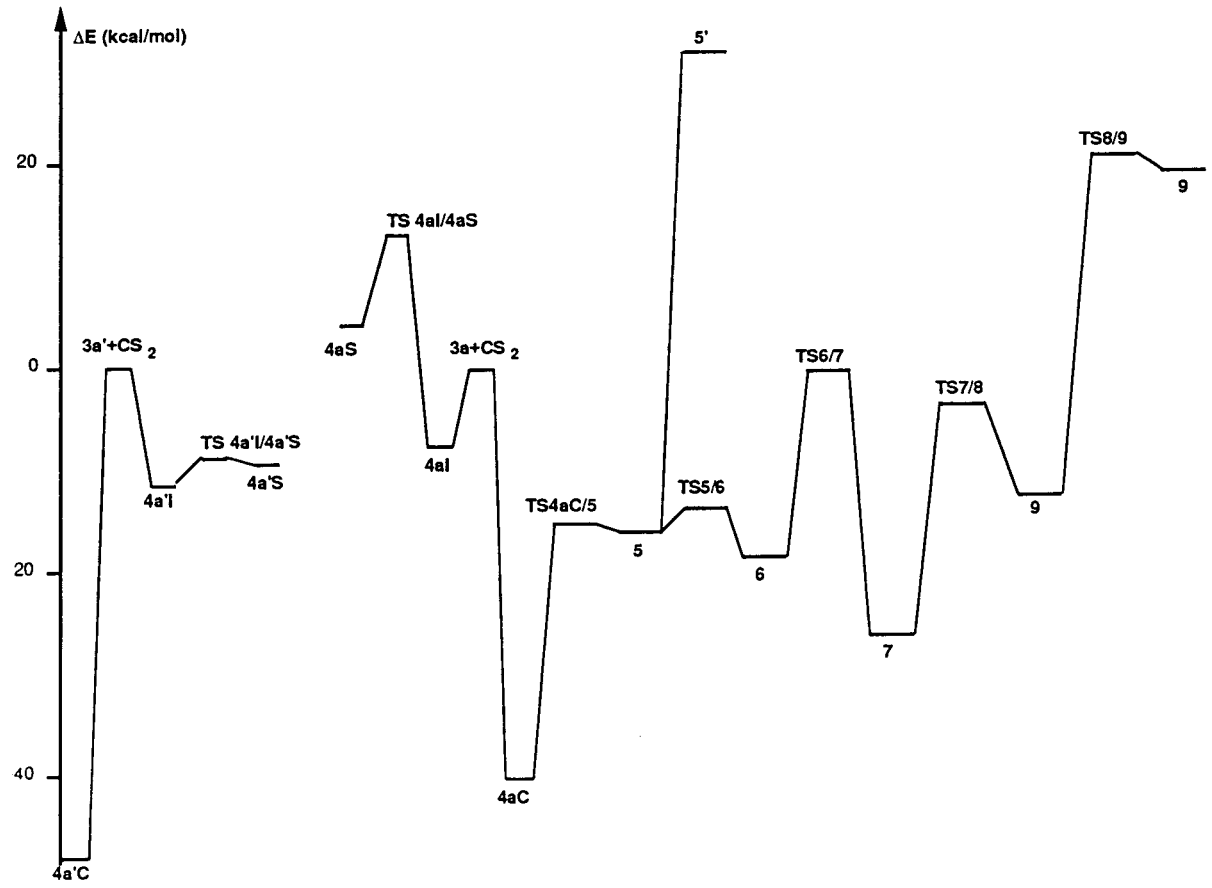

Figure 7. Addition reaction of **3a** (**3a′**) + CS_2 and rearrangement of **4aC** (**4a′C**): scheme of the reaction profile at the B3LYP/6-311+G(2df,2p) + ZPE level of theory. The energies values are relative to those of the reactants.

of the endothermic step **1m** → **2m** that the H_m−C distance is longer (1.450 Å) and the H_m−O distance shorter (1.197 Å). **TS1a′/2a′**, **TS1o/2o**, and **TS1m/2m** (MP2 values in parentheses) lie at 0.4(2.8), 1.5(3.8) and 3.3(6.7) kcal/mol, respectively, above the corresponding reactant complexes. After inclusion of ZPE correction, only the energy barrier of the **1m** → **2m** step remains at the B3LYP level of calculation; in addition, this latter step is the more endothermic process. Thus, the anion obtained by loss of a water molecule to **2m** would be a minor product; consequently, the addition of this anion (**3m**) to CS_2 has not been examined in this work.

Relevant properties of the naked anions are also summarized in Table 1.

The most stable anion is **3a** and H_a is the more acidic labile proton. As mentioned in the Introduction, the stability of **3a** has been attributed to $LP_{Ca} \rightarrow \sigma^*_{S-C(cycle)}$ vicinal delocalization. Our calculations confirm this interpretation: the corresponding interaction energy is −12.9 kcal/mol, and sizable modifications in bond lengths resulting from this delocalization can be noticed. Thus, with respect to **3a′** (for which this delocalization is not allowed), the C_a−S distance is shortened (1.802 vs 1.917 Å), while the S−C_{cycle} distance is lengthened (1.808 vs 1.763 Å). The conversion **3a** → **3a′** is easy (1.0 kcal/mol energy barrier), corresponding to the inversion of the sulfur atoms and takes place prior to unimolecular dissociation. **3o** and **3m** are calculated at our higher level of calculations to be less stable than **3a** by 15.1 and 20.4 kcal/mol, respectively. NPA atomic charges (electron unit) indicate high electron density on the anionic carbon center in **3a** (−0.938) and to some degree in **3a′** (−0.846); in contrast, the charges on the anionic centers in **3o** and **3m** are much less negative (−0.334 and −0.337, respectively). However, these results cannot be attributed to large changes in anionic carbon lone-pair delocalization: the occupancy of the NBO's describing these lone-pairs are 1.817 (**3a**), 1.965 (**3a′**), 1.816 (**3o**), and 1.851 (**3m**).

B. Nucleophilic Addition of 3a and 3a′ to CS_2 and Dissociation of Addition Products. We first examine the approach of the reactants to form the anionic products. The stationary points located on this portion of the potential energy surface are shown in Figure 6, and their energies are given in Table 2. The energetic profile of these nucleophilic additions is illustrated Figure 7.

For both **3a** and **3a′,** two entrance channels have been found. In the first, the CS_2 molecule approaches perpendicularly to the direction of the hybrid lone-pair located on C_a. It is noteworthy that for larger intermolecular distances, the CS_2 approach occurs perpendicularly to the σ_h symmetry plane of the anion (i.e, the same orientation as that found in the product **4aC** (see Figure 6)). This approach is barrierless, and the formation of adducts **4aC** and **4a′C** is very exothermic (−39.5 and −47.8 kcal/mol, respectively, including ZPE correction). **TS4aC/4a′C** connects these two adducts, is reached for an almost planar five-membered ring, and lies only 1 kcal/mol above **4a′C**; the barrier disappears when ZPE correction is added. Consequently, we further examine only the rearrangement of **4aC**.

In the second channel, CS_2 remains in the σ_h plane, and a S atom is directed toward the lone pair of the anionic center; this approach leads to the associations **4aI** and **4a′I** obtained for intermolecular C−S distances of 2.830 and 2.484 Å, respectively (Figure 6). Despite the large intermolecular distances, the neutral CS_2 is fairly bent (CSC bond angle, 169.9° (**4aI**) and 161.1°-(**4a′I**)). NPA analysis indicates a substantial amount of charge transfer from the anion to CS_2: 0.235 eu (**4aI**) and 0.392 eu (**4a′I**), which can be attributed to the $LP_{Ca} \rightarrow \pi^*_{CS2}$ delocal-

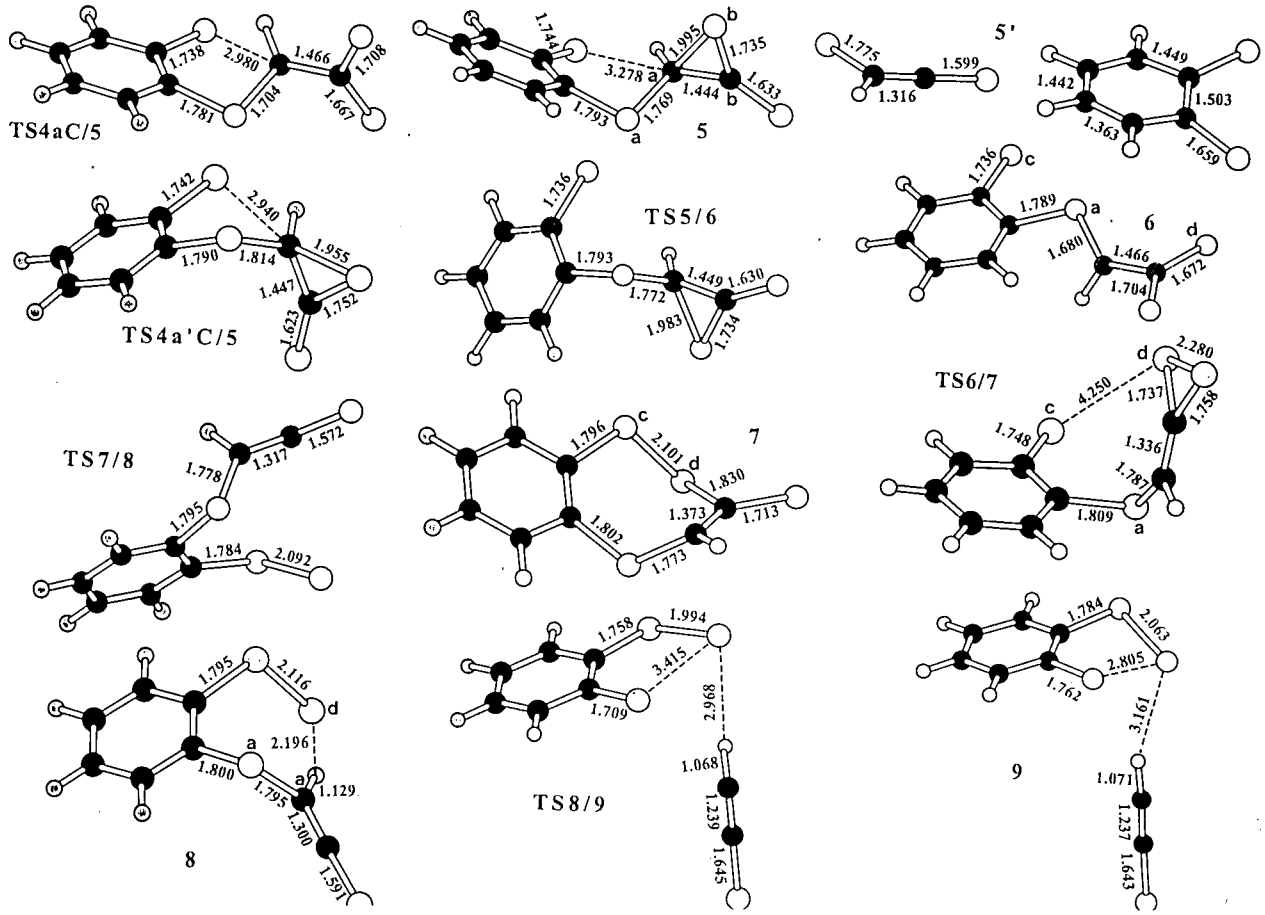

Figure 8. Optimized structures of the stationary points governing the rearrangement of **4aC** (**4a′C**); the distances are in Å.

ization. As shown in Figure 7, the anion adducts **4aS** and **4a′S** have been obtained through **TS4aI/4aS** and **TS4a′I/4a′S**, with energy barriers (including ZPE correction) of 20.9 and 2.8 kcal/mol, respectively. These two steps are calculated to be endothermic by 11.5 and 2.4 kcal/mol, respectively. The thiophilic addition of **3a** to CS_2 is a rather difficult process because CS_2 is syn in **4aI** and anti in **TS4aI/4aS** and **4aS** (the syn thiophilic adduct cannot be found). The energy profile depicted Figure 7 leads us to consider adducts **4aS** and **4a′S** as minority products of addition, and therefore, we examine now only the rearrangement and the fragmentation of **4aC** (or **4a′C**).

Figure 8 displays B3LYP/6-31+G(d)-optimized geometries relevant to the unimolecular process of rearrangement of **4aC**

Direct five-membered C−S bond breaking through the transition structure **TS4aC/5** leads to the intermediate **5** (starting from **4a′C**, the intermediate **5** is also reached through the transition structure **TS4a′C/5**). The formation of **5** is endothermic by 24.6 kcal/mol and occurs with an energy barrier of 26.3 kcal/mol. The three-membered ring in **5** is confirmed by NBO analysis: natural localized molecular orbitals/natural population analysis (NLMO/NPA) bond order of C_a-S_b and C_b-S_b (see Figure 8) are, respectively, 0.756 and 1.036. The fragmentation of **5** by C_a-S_a bond breaking leads to **5′**, i.e., $C_6H_4S_2$ and the anion $S{=}C{=}CHS^-$ (during the elongation of the C_a-S_a bond, the formation of the C_a-S_b double bond is completed, and the C_b-S_b bond is broken). This anion has been detected under NICI by mass spectrometry. By rotation around C_a-C_b, the almost planar intermediate **6** is reached through **TS5/6**. The best Lewis structure of **6** (which presents some conjugation) resulting from a NBO search is indicated in Scheme 5.

TS5/6 lies only 2.8 kcal/mol above **5**, and **6** is more stable than **5** by 2.5 kcal/mol. Our calculations agree with the hypothesis that a cyclic form **7** (named **a** in Scheme 3) is a viable intermediate, which results from the rearrangement of **4aC**, because we have succeeded in locating a transition stucture, **TS6/7**, that connects **6** and **7**. **TS6/7** is reached by rotation around the $C-S_a$ bond of **6**; this rotation causes a substantial change of the $HCCS_2$ fragment, which possesses a dithiacyclopropylvinylidene structure (NLMO/NPA C=C and S−S bond orders are, respectively, 1.864 and 0.897, the negative charge being localized essentially on S_c (see Figure 8)). At the same time, the S_c-S_d distance is reduced from 6.0 to 4.25 Å. **7** is calculated to be more stable than **6** by 7.6 kcal/mol, and **TS6/7** lies 17.9 kcal/mol higher than **6**. This barrier is not too high, and the formation of **7** seems feasible under experimental conditions. It is expected that the competitive fragmentations of **7** can lead to both the $HCCS^-$ and $HC_2S_2^-$ anions (see Scheme 3). However, despite an extensive search, we were unable to find a reaction pathway to give rise to the formation of the latter anion. On the other hand, the rearrangement of **7** by S_d-C bond breaking leads to intermediate **8**, characterized by the presence of a thioketene group and a S_d-H hydrogen bond (NLMO/NPA bond order equals 0.051). This **7** → **8** step occurs with an energy barrier of 22.6 kcal/mol, and it is endothermic (13.6 kcal/mol). At this point, no viable restricted (R)B3LYP pathway was found in which S_a-S_d bond forming and S_a-C_a bond breaking occur. An alternative is offered through unrestricted (U)B3LYP calculations: a diradical intermediate **9** has been located and explains the presence of the $HCCS^-$ anion. **9** lies 31.5 kcal/mol above **8**. Because $S^2 = 0.85$ for this reaction intermediate, it is a mixture of 57% pure singlet

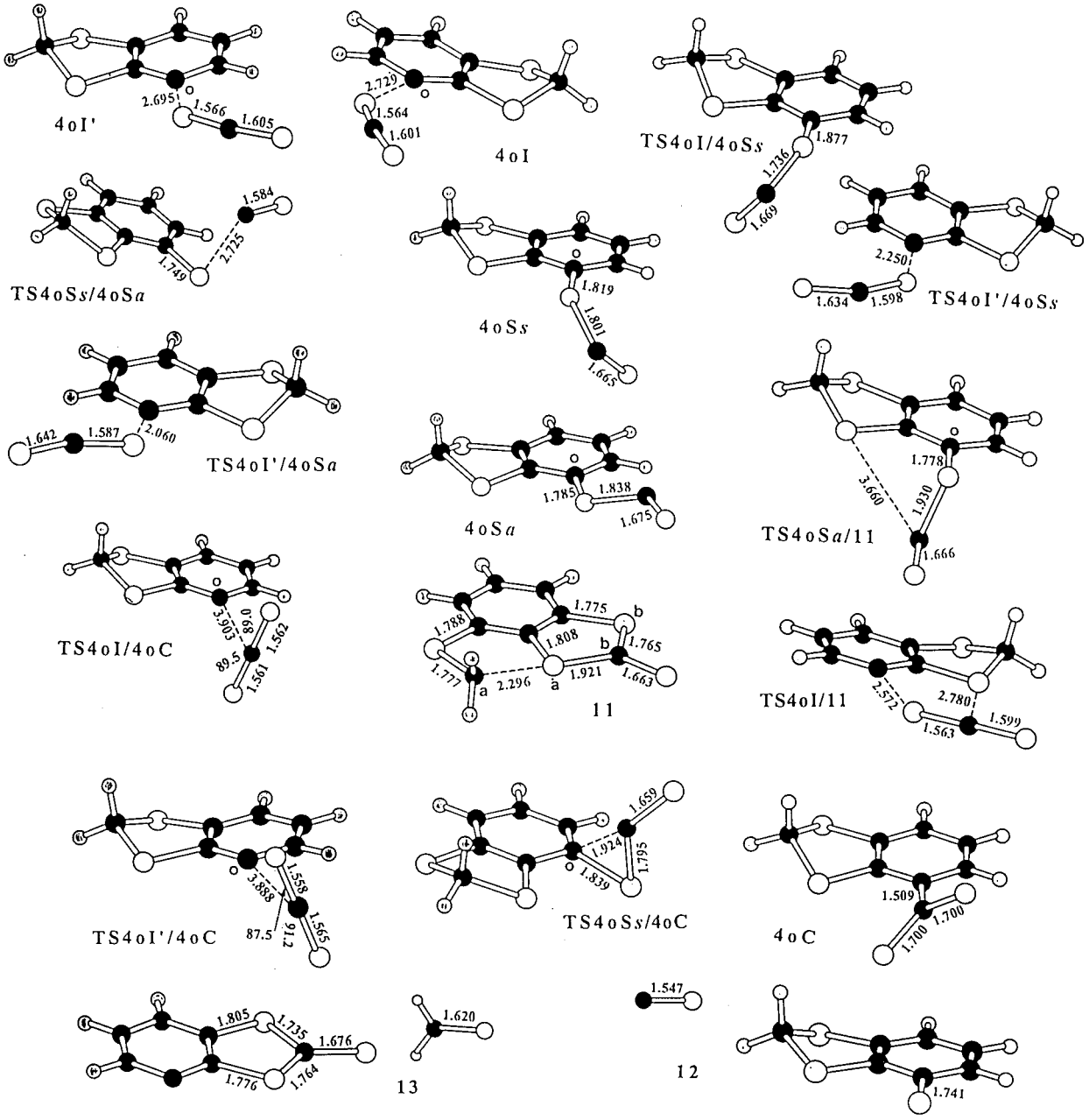

Figure 9. Optimized structures of the stationary points governing the **3o** addition to CS_2; the distances are in Å

SCHEME 5

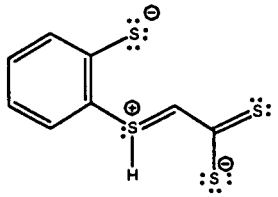

($S^2 = 0$) and 43% pure triplet ($S^2 = 2$) states; the computed energy is a weighted average of these two states (23). At the optimized geometry of **9**, the triplet (U)B3LYP energy ($S^2 = 2.01$) is 0.5 kcal/mol lower than that of the mixed ($S^2 = 0.85$) spin state. Consequently, the energy correction for the diradical with $S^2 = 0$ should be only 0.4 kcal/mol higher than that of this mixed state. **TS8/9**, which connects **8** and **9**, is also diradical in character ($S^2 = 0.79$); the triplet energy ($S^2 = 2.01$) is, in this case, 1.5 kcal/mol higher than that of the mixed spin state; the energy correction lowers the energy barrier by 1.0 kcal/mol to 30.5 kcal/mol. This value does not seem prohibitive for the formation of $HCCS^-$.

C. Nucleophilic Addition of 3o to CS_2. The stationary points located on the CS_2/**3o** potential energy surface are shown in Figure 9, and their energies are given in Table 3. Finally, the energetic profile of this addition is illustrated in Figure 10.

Unlike α-anion addition, geometry optimizations starting at large intermolecular distances and for different approaches of the reactants systematically led to the precomplexes **4oI** (or **4oI′**). In particular, a CS_2 approach perpendicular to the plane of the aromatic six-membered ring does not correspond to a minimum-energy pathway. Therefore, **4oI** (or **4oI′**) plays a determining role in the orientation of the reaction because in these associations, a C_o-S bond is in the process of being made (NLMO/NPA bond order ~0.1). In the two cases, CS_2 is bent (SCS bond angle ~169°) and adopts a syn conformation. These two precomplexes lie 9.5 kcal/mol below the reactants. As mentioned above, the **3o** anion does not add directly the carbon atom of CS_2. However, starting from these precomplexes, an

TABLE 3: Energies and Zero-Point Energies (relative to those of the reactants) for the Stationary Points on the 3o + CS_2 Potential Surface Depicted in Figure 10[a]

systems	ΔE	ΔZPE	systems	ΔE	ΔZPE
4oI	−9.9	0.5	**TS4oI/11**	−0.6	0.8
4oI′	−10.0	0.5	**11**	−20.2	0.8
TS4oI/4oS*s*	−8.0	0.9	**TS4oI/4oC**	−1.2	0.1
TS4oI′/4oS*s*	−8.5	0.7	**TS4oI′/4oCs**	−1.2	0.0
4oS*s*	−10.9	1.0	**TS4oSs/4oC**	16.7	0.3
TS4oS*s*/4oS*a*	−3.2	0.4	**4oC**	−57.6	2.9
TS4oI′/4oS*a*	−12.6	1.3	**12**	−1.2	−0.1
4oS*a*	0.5	0.7	**13**	8.9	−1.8
TS4oS*a*/11	−7.9	0.9			

[a] Energies in kcal/mol.

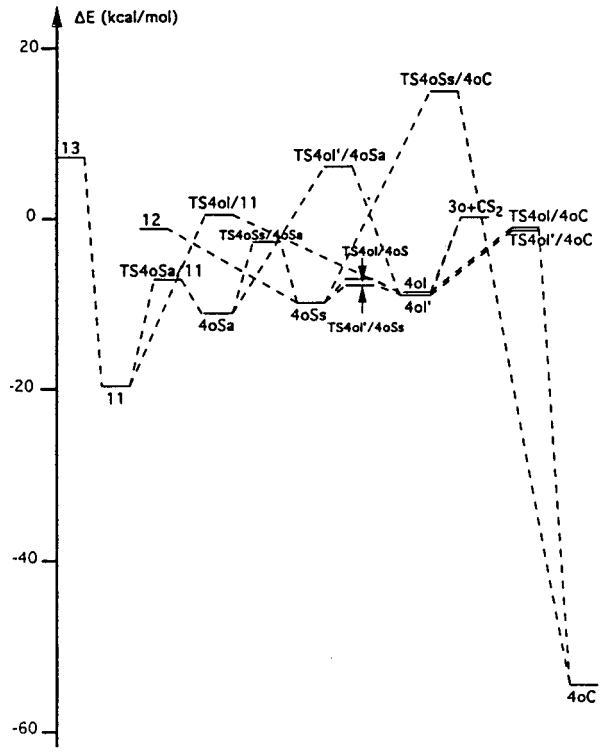

Figure 10. Addition reaction **3o** + CS_2: scheme of the reaction profile at the B3LYP/6-311+G(2df,2p) + ZPE level of theory. The energies values are relative to those of the reactants.

increase of C_oCS angle (see Figure 9) leads to the **TS4oI/4oC** and **TS4oI′/4oC**, respectively, which evolve toward the adduct **4oC**. Despite the large exothermicity of this step, the barrier height is calculated to be 8.1 kcal/mol, a value ∼6.5 kcal/mol higher than the barrier calculated for the **4oI**(**4oI′**) → **4oS*s*** step. On the basis of this result, **4oSs** will be the main kinetic product. It is a typical case where a kinetic control orients the process. This means that the carbophilic attack is always unfavored at the ortho site, in contrast to the thiophilic approach, even if it is less exothermical. In the following, we focus our attention only on the rearangement of **4oSs**.

4oI (and **4oI′**) leads to the syn adduct **4oSs**; the **4oI**(**I′**) → **4oSs** step is barely exothermic (0.5 kcal/mol), with a low energy barrier (1.6 kcal/mol). The anti adduct **4oSa** is more stable than the syn by 1.5 kcal/mol and located for a slightly longer C_o-S distance. The transition state **TS4oSs/4oSa** that connects the two adducts was found to be 7.1 kcal/mol higher than **4oSs** and located for a large C−S distance (see Figure 9). This result suggests that fragmentation of **4oSs** into **12** is a rather easy process. Another evolution of **4oSs** occurs by rotation around the C_o-S bond and shortening the $C_o-C(S_2)$ distance to give **4oC** through **TS4oSs/4oC**. But **TS4oSs/4oC** was found to be 23.5 kcal/mol higher than **4oSs**; thus this alternative pathway is disfavored, despite its large exothermicity. Figure 10 shows that a direct pathway leads to **4oSa**, which starts from **4oI′**. The energy barrier of this direct pathway is 10.7 kcal/mol, and thus, it is somewhat less favored than the two-step route. As for **4oSa** formation, two ways have been established to reach the intermediate **11**: by rotation around the C_o-S bond of **4oSa** (the corresponding transition state **TS4oSa/11** lies only 4.3 kcal/mol higher than **4oSa**) and by migration of the CS_2 moiety of **4oI** toward a S atom of the five-membered ring, with an energy barrier of 9.0 kcal/mol. Figure 10 shows that this pathway is not as easy as the first. In the bicyclo intermediate **11**, the negative charge is localized essentially on C_a, despite an important $LP_{Ca} \rightarrow \sigma^*_{Sa-Cb}$ delocalization (occupation of LP_{Ca}: 1.622 instead of 2.0). This delocalization results in a weak C_a-S_a bond (NLMO/NPA bond order equal to 0.222); the S_a-C_b bond also becomes weaker (NLMO/NPA bond order equal to 0.633 instead of 1.006 for the S_b-C_b bond). As suggested in Scheme 3, the fragmentation of **11** leads to **13**, which lies 30.1 kcal/mol above **11**.

Conclusion

We have investigated the reactivity of carbanions derived from 1,3-benzodithiole bisdeuterated at C_2 toward carbon disulufide. Under NICI conditions, we have prepared two nonconverting carbanions: the first resulting from an abstraction of an *o*-aromatic proton and the second by abstraction of a deuteron. Results obtained from DFT calculations are consistent with the experimental observations:

(i) the dithioacetal anion reacts with CS_2 at the carbon, while the *o*-aromatic anion reacts at the sulfur;

(ii) the mechanism proposed for the formation of the main fragments produced under CID conditions has been confirmed by calculation. In addition, for the postulated intermediate **7**, calculations have suggested a mechanism of fragmentation in good agreement with experimental results.

Acknowledgment. The authors are indebetd to A. Spote and R. Rosenberg for their experimental skills. We thank the FNRS (Belgium), the CNRS, and the DRED (France) for support. A generous allocation of computer time by the CINES is also gratefully acknowledged.

Supporting Information Available: BSS corrections at B3LYP level using 6-31+G(d) and 6-311+G(2df,2p) basis set (Table A); absolute energies and zero-point vibrational energies for all stationary points on the potential surfaces at all levels of calculations (Tables B−E). This material is available free of charge via the Internet at http://pubs.acs.org.

References and Notes

(1) Bernardi, F.; Czizmadia, I. G.; Mangini, A. *Organic Sulfur Chemistry*, Elsevier: Amsterdam, 1985.

(2) (a) Epiotis, N. D.; Yates, R. L.; Bernardi, F.; Wolfe, S. *J. Am. Chem. Soc.* **1976**, *98*, 5435. (b) Lehn, J. M.; Wipff, G. *J. Am. Chem. Soc.* **1976**, *98*, 7498.

(3) Seebach, D. *Synthesis.* **1969**, 17.

(4) Noube, S.; Pelter, A.; Smith, K.; Blatcher, P. *Tetrahedron Lett.* **1978**, *26*, 2345.

(5) Kundig, E. P.; Cunningham, A. J. *Tetrahedron* **1988**, *44*, 6855.

(6) Moradpour, A.; Bittner, S.; Bernstein, J.; Sarma, J. A. R. P. *J. Chem. Soc., Perkin Trans 1* **1988,** 2751.

(7) Gimbert, Y.; Moradpour, A.; Bittner, S.; Jordis, U. *Tetrahedron Lett.* **1989**, *30*, 819.

(8) (a) Bartmess, J. E.; Hays, R. L.; Khatri, H. N.; Misra, R. N.; Wilson, S. R. *J. Am. Chem. Soc.* **1981**, *103*, 4746. (b) Gimbert, Y.; Arnaud, R.; Tabet, J. C.; De Hoffmann, E. *J. Phys. Chem.* **1998**, *102*, 3732.

(9) (a) Ingemann, S.; Kleingeld, J. C.; Nibbering, N. M. M. In *Ionic Processes in the Gas Phase*; Ferreira, M. A. A., Ed.; Reidel: Dordrecht, The Netherlands, 1984; p 87. (b) DePuy, C. H.; Bierbaum, V. M. *Acc. Chem. Res.* **1981**, *14*, 146. (c) Gronert, S.; O'Hair, R. A.; Prodnuck, S.; Sülzle, D.; Damrauer, R.; DePuy, C. H. *J. Am. Chem. Soc.* **1990**, *112*, 997.

(10) Frisch, M. J.; Trucks, G. W.; Schlegel, H. B.; Scuseria, G. E.; Robb, M. A.; Cheeseman, J. R.; Zakrzewski, V. G.; Montgomery, J. A.; Stratmann, R. E., Jr.; Burant, J. C.; Dapprich, S.; Millam, J. M.; Daniels, A. D.; Kudin, K. N.; Strain, M. C.; Farkas, O.; Tomasi, J.; Barone, V.; Cossi, M.; Cammi, R.; Mennucci, B.; Pomelli, C.; Adamo, C.; Clifford, S.; Ochterski, J.; Petersson, G. A.; Ayala, P. Y.; Cui, Q.; Morokuma, K.; Malick, D. K.; Rabuck, A. D.; Raghavachari, K.; Foresman, J. B.; Cioslowski, J.; Ortiz, J. V.; Stefanov, B. B.; Liu, G.; Liashenko, A.; Piskorz, P.; Komaromi, I.; Gomperts, R.; Martin, R. L.; Fox, D. J.; Keith, T.; Al-Laham, M. A.; Peng, C. Y.; Nanayakkara, A.; Gonzalez, C.; Challacombe, M.; Gill, P. M. W.: Johnson, B.; Chen, W.; Wong, M. W.; Andres, J. L.; Gonzalez, C.; Head-Gordon, M.; Replogle, E. S.; J. A. Pople. *Gaussian 98*, Revision A.6; Gaussian, Inc.: Pittsburgh, PA, 1998.

(11) Frisch, A. E.; Frisch, M. J. *Gaussian 98 User's Reference*; Gaussian, Inc.: Pittsburgh, PA, 1998.

(12) Becke, A. D. *Phys. Rev. B* **1988**, *38*, 3098.

(13) Lee, C.; Yang, W.; Parr, R. G. *Phys. Rev. B* **1988**, *37*, 785.

(14) For a review, see: Reed, A. E.; Curtiss, L. A.; Weinhold, F. *Chem. Rev.* **1988**, *88*, 899.

(15) Wiberg, K. B.; Rablen, P. R. *J. Comput. Chem*, **1993**, *14*, 1504.

(16) ^{34}S experiments from $[\mathbf{1}_{d2}-D]^-$ and $[\mathbf{1}_{d2}-H]^-$ ions and, furthermore, the fact that CS_2 in the collision cell contains natural ^{34}S isotopes (any ion containing sulfur atoms from CS_2 must be accompanied by a peak 2 au higher, whose intensity has to be 4% per S atom from CS_2) allowed us to determine on the number and origin of sulfur atoms into the different ions produced.

(17) The formation of the different deprotonated forms of 1,3-benzodithiole $\mathbf{1}_{d2}$ seemed to be dependent on the gas-phase reagent (i.e., ammonia, diethylamine, methanol, and the N_2O/CH_4 mixture) used in the high-pressure source. Investigations regarding the strength of the gas-phase reagent used under NICI conditions showed that the ion abundance ratio (*m*/*z* 154)/(*m*/*z* 155) increased significantly when weaker bases were used.

(18) (a) Ingemann, S.; Nibbering, N. M. M. *Can. J. Chem.*, **1984**, *62*, 2273. (b) Binkley, R. W.; Flechtner, T. W.; Tevesz, M. J. S.; Wimik, W.; Zhong, B. *Org. Mass. Spectrom.* **1993**, *28*, 769.

(19) (a) Graul, S. T.; Squires, R. R. *J. Am. Chem. Soc.* **1989**, *111*, 892, and references therein. (b) DePuy, C. H.; Bierbaum, V. M.; Damrauer, R.; Soderquist, J. A. *J. Am. Chem. Soc.* **1985**, *107*, 3385. (c) Froelicher, S. W.; Freiser, B. S.; Squires, R. R. *J. Am. Chem. Soc.* **1986**, *108*, 2853. (d) Sheldon, J. C.; Bowie, J. H.; DePuy C. H.; Damrauer, R. *J. Am. Chem. Soc.* **1986**, *108*, 6794.

(20) The counterpoise method of Boys and Bernardi[21] has been used to estimate BSSE of some representative sysems investigated in this work; results are collected in Table A (Supporting Information). Concerning nucleophilic addition to CS2, the B3LYP/6-311+G(2df, 2p) basis set is essentially BSSE-free; this result suggests that single-point calculations using this basis set provide an effective procedure for nucleophilic additions. For proton tranfer reactions, BSSE is almost the same regardless of the basis set used and the nature of the stationnary points. In this case, correction for BSSE could be necessary, but the relative energies cannot be altered.

(21) Boys, S. F.; Bernardi, F. *Mol. Phys.* **1970**, *19*, 553.

(22) MP2 relative energies are hadly sensitive to the choice of geometry; for instance, the use of MP2/6-31G(d) optimized geometries leads to relative energies (kcal/mol) of −19.0 (**1o**), −14.9 (**TS1o**/**2o**), and −17.8 (**2o**), values very close to those obtained using B3LYP geometries (see Table 1). Thus, only MP2/6-31+G(d)//B3LYP/6-31+G(d) calculations have been performed for all stationnary points of the proton-transfer surfaces.

(23) (a) Yamaguchi, K.; Jensen, F.; Dorigo, A.; Houk, K. N. *Chem. Phys. Lett.* **1988**, *149*, 537. (b) Yamanaka, S.; Kawakami, T.; Nagao, H.; Yamaguchi, K. *Chem. Phys. Lett.* **1994**, *231*, 25.